13th International Symposium on Turbulence and Shear Flow Phenomena (TSFP13)
Montreal, Canada, June 25-28, 2024

Coherent Wave Generation in Swept-Wing Boundary Layer Transition at a Real Flight Condition

Yuji Mori
Department of Aerospace Engineering
Tohoku University
6-6 Aramaki Aza Aoba, Aoba-ku,
Sendai, Miyagi 980-8579, Japan
yuji.mori.r6@dc.tohoku.ac.jp

Aiko Yakeno
Institute of Fluid Science
Tohoku University
2-1-1 Katahira, Aoba-ku,
Sendai, Miyagi 980-8577, Japan
aiko.yakeno@tohoku.ac.jp

Shigeru Obayashi
Institute of Fluid Science
Tohoku University
2-1-1 Katahira, Aoba-ku,
Sendai, Miyagi 980-0857, Japan
s.obayashi@tohoku.ac.jp

ABSTRACT

We conducted numerical investigations of transitions from laminar to turbulent over a swept wing exposed to artificial disturbances such like surface roughness (SR) or/and free-stream turbulence (FST). Our primary focus was on boundary layer receptivity and growth process of induced unstable waves at a real flight condition. We developed the computation technique to simulate a transition from laminar to turbulent over a real swept wing. The Reynolds number, based on the mean aerodynamic chord, is 17,500,000, the free-stream Mach number is 0.86, and the angle of attack is 1.5 [deg]. We first operated the RANS for the NASA Common Research Model with natural laminar flow (CRM-NLF), which applies a new NLF design method developed at NASA Langley Research Center. We operated precise simulations around the wall surface and caused transition using artificial disturbances such as the wall surface roughness and the free-stream turbulence. We confirmed the stationary and even traveling coherent wave generation and their responses to the artificial disturbances even at the real flight condition.

BACKGROUND AND OBJECTIVE

Modern aircraft commonly employ swept wings to delay the onset of shock waves. To improve the aerodynamic performance of aircraft with such swept wings, reducing frictional drag has been raised as one of the last resorts. Turbulence increases the friction drag, "Laminarization," which suppresses the increase in turbulent energy during transition, is once again in the spotlight (Schrauf, G. (2005), Arnal, D., Archambaud, J. P., (2008)).

It has been unclear what transition mechanism was dominant to cause transition around a swept-wing (Poll, D. I. A. (1985), Saric, W. S., (1994), Reed, H. L., Saric, W. S., Arnal, D. (1996), Reed, H. L., Saric, W. S. (2008)). At least several unstable solutions known from classical linear stability analysis have been attempted to explain transition around a swept wing; the Tollmien-Schlichting (TS), crossflow (CF), attachment line, and Görtler instabilities. However, from our studies (Yakeno, A., Obayashi, S. (2021)), when targeting an actual main wing, such a classical stability analysis is insufficient because it assumes an ideal state too much and it does not explain the phenomena that occur. In reality, the unstable modes grow in parallel and interact with each other, whether one of them becomes dominant in the transition depends on the conditions of the atmospheric

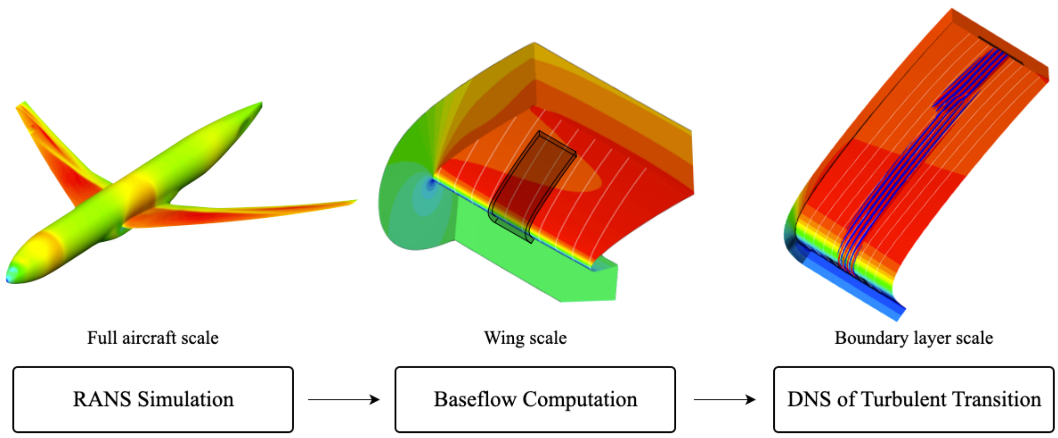

Figure 1. Concept of our "Inverse Hybrid Computation".
DNS for transitions near the wall and RANS simulation for surrounding flow, over a real aircraft under an actual cruising condition.

turbulence and the roughness of the wall surface (Mori, Y., Yakeno, A., Obayashi, S. (2024)).

Similarly, there are other performance tests that are now considered insufficient. For example, DRE and its derivative laminar flow devices have been considered (Saric, W. S. *et al.* (1998, 2019), Ide, Y. *et al.* (2021), Hirota, M. *et al.* (2019)), but when applied to actual aircraft, DRE does not fully demonstrate the performance confirmed in wind tunnel experiments under low-speed conditions (Saric, W. S., West, D. E., Tufts, M. W., Reed, H. L. (2015)). The reason for this is that the conventionally well-known stationary wave, which is the target of DRE, is not sufficient as the unstable mode to be considered. In fact, several research teams have pointed out that in the case of large aircraft, the turbulent boundary layer generated from the fuselage causes turbulent airflow to enter the leading edge of the swept wing (Gaster, M. (1967), Poll, D.I.A. (1979)). Depending on the frequency band of the turbulent airflow, not only stationary waves but also traveling waves are generated, which may even increase nonlinear motion further upstream from the point where the stationary waves become unstable (Mori, Y., Yakeno, A., Obayashi, S. (2024)). Thus, the transition around a swept wing is influenced by various factors. To reduce frictional drag, it is necessary to further understand such complex transition phenomena, and testing under actual aircraft cruising conditions is essential.

Recent advances in computation technology provides further understanding of flow around the real aircraft, which has been by using the Reynolds-averaged Navier-Stokes equations (RANS) model. RANS simulation is an excellent tool that offers convergent solutions hundreds to thousands of times faster than DNS, but generally it is difficult to predict flow separation and reattachment, because RANS cannot predict transitions as is due to the nature of its governing equation. Therefore, although we use RANS for the surrounding flow, we needed to be able to predict transitions under actual cruising conditions by analyzing near walls using DNS.

In this study, we conducted DNSs of laminar-turbulent transition over a swept wing of a transonic aircraft under a real flight condition. The baseflow is derived from the flow around the entire aircraft computed using RANS simulation. The validity of this inverse hybrid method was confirmed by comparison with the results of a wind tunnel experiment conducted under similar conditions. Finally, the transition was triggered by introducing artificial disturbances to the baseflow, in the same way as in our previous study (Mori, Y., Yakeno, A., Obayashi, S. (2024)).

PREPARATION FOR TRANSITION COMPUTATION

Flow Configuration

We investigated the flow around the NASA Common Research Model with natural laminar flow (CRM-NLF), which applies a new NLF design method developed at NASA Langley Research Center (Lynde, M. N., Campbell, R. L., (2017)). For comparison, our computation was operated at the same condition as Paredes and Venkatachari (2021) demonstrated experimentally at the National Transonic Facility (NTF). The Reynolds number, based on the mean aerodynamic chord, is 17,500,000, the free-stream Mach number is 0.86, and the angle of attack is 1.45 [deg].

For DNSs of turbulent transition in this study, RANS simulation and DNS were utilized separately depending on the scale of the computational domain, as shown in Figure 1. First, the flow around the swept wing was computed, considering the three-dimensional shape of the wing and the presence of the fuselage (left in Figure 1). Given the necessity for a large-scale calculation of the entire aircraft model, a steady RANS simulation was employed for a relatively cost-effective analysis. However, the obtained flow exhibited turbulence due to eddy viscosity from the turbulence model, resulting in disparities from laminar flow. Then, DNS was conducted on a portion of the wing using the RANS results to compute the baseflow (middle in Figure 1). Finally, a high-resolution DNS transition analysis was conducted for the vicinity of the boundary layer. With the baseflow as the initial field, a transition was triggered by applying artificial disturbances, as mentioned later (right in Figure 1). All the results in this study were obtained using an in-house solver, LANS3D. Details of the computational setup in each step are described below sections.

RANS Computation

As a first step, we performed a steady RANS simulation for the CRM-NLF semi-span model. The turbulence model was the standard Spalart-Allmaras one-equation model (Spalart and Allmaras (1994)). We utilized the structural grid provided in *the 1st AIAA CFD transition modeling and prediction workshop*. The

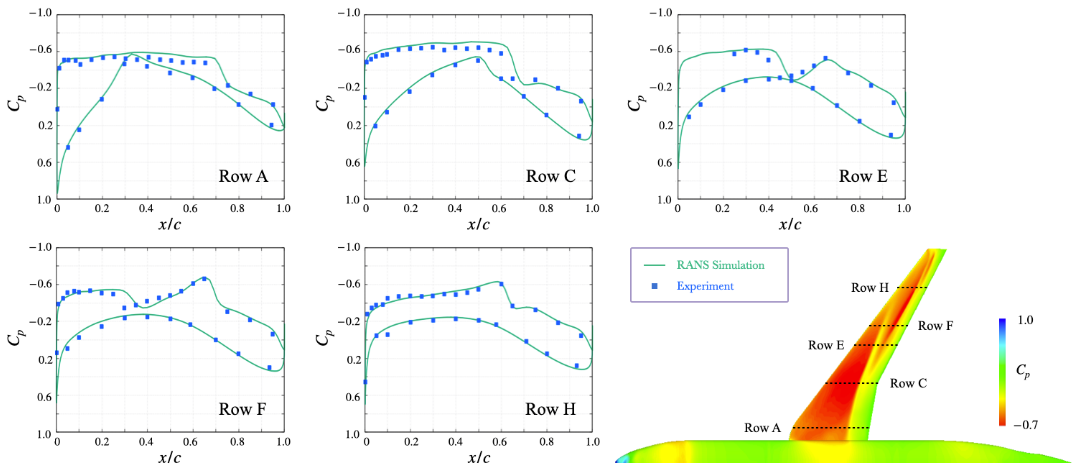

Figure 2. Comparison of the present RANS computation and wind tunnel experimental results (Paredes and Venkatachari (2021)) of distribution of pressure coefficient C_p over the wing surface at five spanwise positions of CRM-NLF model.

computational grid comprises five body-fitted grids surrounding the aircraft surface and three rectangular grids covering the entire aircraft, totaling approximately 6.4 million grid points. Numerical fluxes for RANS equations were evaluated using a second-order upwind scheme with the Monotonic Upwind Scheme for Conservation Laws (MUSCL) scheme (B. van Leer (1979)). The modified van Albada flux limiter (Kermani, M., Gerber, A. and Stockie, J., (2003)) was applied to avoid spurious oscillations due to shock wave discontinuities. To alleviate the severe time step constraint, we employed the implicit ADI-SGS method for the time integration (Nishida, H. and Nonomura, T. (2006)). Boundary conditions were set as follows: a free-stream condition for the far-field boundary, a symmetric boundary condition for the symmetry plane of the CRM-NLF model, and non-slip and adiabatic conditions for the wall surface.

The comparison of the present RANS computation and wind tunnel experiment results (Paredes and Venkatachari (2021)) of distribution of pressure coefficient C_p over the wing surface at five spanwise positions of CRM-NLF model is shown in Figure 2. The horizontal axis is the distance from the leading edge in the streamwise direction, and the vertical axis is the pressure coefficient. Except for slight differences in the vicinity of the shock wave, the RANS computational results are in very good agreement in experimental results for all cross-sections.

Baseflow Computation

Next, a baseflow (non-disturbed steady flow) was computed for a part of the swept wing using RANS simulation results. The results of linear stability analysis by Lynde, Cambell and Viken (2019) indicate that what transition mechanism governs the transition depends on flow conditions and position on the wing surface. In this paper, we will introduce an analysis example that focuses on crossflow (CF) instability, which is one of a typical transition process around swept wings. At the present Reynolds number, and the angle of attack, the CF instability becomes dominant in the region on the wing tip side.

Thus, the computational domain was chosen to be the wing tip side, as this study primarily addresses transitions caused by CF instability. Given the unsteady flow downstream of the shock wave due to separation, the region was up to a slightly upstream of the shock wave. The body-fitted coordinate system (ξ, η, ζ) was taken to be ξ perpendicular to the leading edge, η in the spanwise direction, and ζ in the vertical direction to the wing surface. The number of grid points in each direction is (ξ, η, ζ) = (141, 85, 96), totaling approximately 1.2 million. The governing equations are the three-dimensional compressible Navier–Stokes (NS) equations, and the numerical scheme was same as the RANS simulation.

The far-field and inflow boundaries were fixed with the RANS solution. For the outflow boundary, only the pressure was fixed with the RANS solution, while the rest (density and velocity) were linearly extrapolated. Non-slip and adiabatic conditions were applied to the wall. By advancing the time step with these computational settings, a steady solution was obtained. Using this flow as the baseflow, we proceeded to the transition analysis. It is noted that, as the inflow boundary is fixed with the RANS solution, the flow near this region is not suitable as a baseflow. To minimize this effect, a relatively large computational domain was taken for the baseflow computation, and the computational domain for the transition analysis was positioned at a distance from the inflow boundary.

TRANSITION COMPUTATION

DNS computation

The body-fitted coordinate system (ξ, η, ζ) was taken to be ξ in the streamwise direction around the wing, η in the sweep direction, and ζ in the vertical direction of the wing surface. The number of grid points in each direction is (ξ, η, ζ) = (683,287, 107), totaling approximately 21 million.

To reduce the computational domain required in the spanwise direction, the grid in the flow direction ξ was aligned with the growth direction of the stationary crossflow waves induced by CF instability. This corresponds to the flow direction near the inflection point in the crossflow velocity profile. A sponge region was introduced near the spanwise boundary. As the boundary layer thickness develops significantly from the leading edge to downstream, the grid spacing in the ζ direction was adjusted accordingly, ensuring that the number of grid points in the boundary layer remains constant at any point.

The governing equations were three-dimensional compressible NS equations. Spatial derivatives of the governing equations were numerically evaluated using a sixth-order compact finite difference scheme (Lele, S. K. (1992)). A tenth-order implicit filtering (Gaitonde, D. V., Visbal, M. R. (2000)) with a free parameter of 0.495 (Kawai, S., Fujii, K. (2008)) was applied to suppress high-frequency numerical oscillations. Time integration employed the third-order TVD Runge–Kutta method (Shu, C. W., Osher, S. (1988)). Boundary conditions were applied to walls with non-slip and adiabatic boundary conditions, and all other boundaries were fixed with baseflow. To prevent spurious reflections and solution divergence at the boundaries, the same kind of filter as used in (Schrader, L. U. *et al*. (2009); Tempelman, D. *et al.* (2012)) was applied around all boundaries.

Artificial Disturbance

The transition was triggered by introducing artificial disturbances to the baseflow, in the same way as in our previous study (Mori, Y., Yakeno, A., Obayashi, S. (2024)). Surface roughness was modelled as an artificial disturbance by placing a lot of local roughness elements with a Gaussian distribution on the wing surface. Each roughness element was given by the following equation.

$$h(X,Y) = D_{sr}\exp\left(-r_{dist}^2/2\sigma^2\right) \tag{2}$$

with

$$r_{dist}^2 = (X-X_c)^2 + (Y-Y_c)^2 \tag{3}$$

Here, (X, Y) is the coordinate system on the wing surface, where X is the coordinate in the direction perpendicular to the leading edge and Y is the coordinate along the leading edge. h is the height of the roughness element at each position, (X_c, Y_c) is the center of the roughness element and σ is the radius of roughness. D_{sr} is the maximum height but changes sing randomly for each roughness element. As the unstable modes in the region where the transition analysis was performed had not been identified, the surface roughness was created to include a wide range of wavenumber components, so that disturbances of various wavenumbers could be introduced. The arithmetic average roughness of the roughness generated was scaled to be approximately 1% of the boundary layer thickness (99% thickness) at the leading edge. We calculated the power spectral density (PSD) in the spanwise direction averaged in the streamwise direction, and confirmed that modes of a wide range of wavenumbers are evenly included.

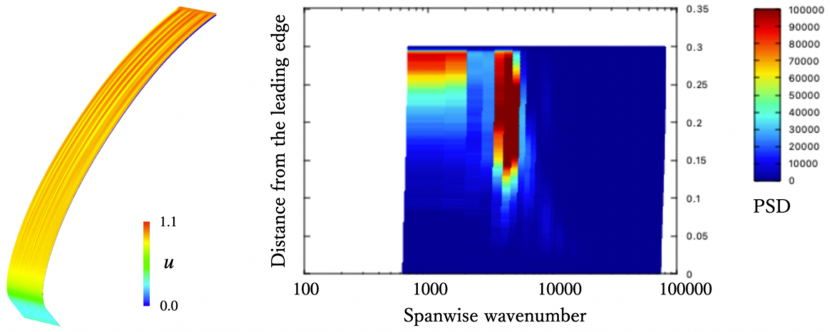

Figure 3 Coherent wave generation after enough time when the surface roughness was applied.
In the left figure, a contour surface colored with the streamwise velocity is shown.
In the right figure, the power spectral density at the inflection point of the mean flow velocity is shown.

DNS Results with the Artificial Disturbance

In this paper, the result when only surface roughness was applied is shown in Figure 3. The velocity distribution in the free- stream direction within the boundary layer (Figure 3 left) and the spanwise wavenumber spectrum in the flow direction are shown (Figure 3 right). Similar to the results in Yakeno, A. and Obayashi, S. (2021) and Mori, Y., Yakeno, A. and Obayashi, S. (2024), traveling waves are generated immediately after applying surface roughness. And, after a sufficient amount of time had passed, it was observed that stationary waves remained. The stationary wave with a spanwise wavenumber of 5000 grew most strongly, and this mode was identified as the unstable mode with only the fixed surface roughness.

ACKNOWLEDGEMENTS

Numerical simulations were performed on the "AFI-NITY" supercomputer system at Institute of Fluid Science, Tohoku University. This work was supported by NEDO of Japan (JPNP20010). A. Y. appreciates the support of the KAKENHI (19K14880, 19KK0373, and 23H01335) from JSPS by MEXT of Japan and JST FOREST Program (JPMJFR222R).

REFERENCES

Schrauf, G., 2005, "Status and Perspectives of Laminar Flow", *Aeronautical Journal*, Vol. 109, No. 1102, pp. 639–644.

Arnal, D., Archambaud, J. P., 2008, "Laminar-turbulent transition control: NLF, LFC, HLFC", *Advances in Laminar-Turbulent Transition Modeling*, AVT-151 RTO AVT/VKI Lecture Series, Brussels, Belgium: Von Karman Inst. for Fluid Dynamics.

Poll, D. I. A., 1985, "Some observations of the transition process on the windward face of a long yawed cylinder", *Journal of Fluid Mechanics*, Vol. 150, pp. 329–356.

Reed, H. L., Saric, W. S., 2008, "Transition Mechanisms for Transport Aircraft", *AIAA Paper*, No. 2008-3743.

Saric, W. S., 1994, "Görtler Vortices", *Annual Review of Fluid Mechanics*, Vol. 26, pp. 379-409.

Reed, H. L., Saric, W. S., Arnal, D., 1996, "Linear stability theory applied to boundary layers", *Annual Review of Fluid Mechanics*, Vol. 28, pp. 389-428.

Yakeno, A., Obayashi, S. 2021, "Propagation of stationary and traveling waves in a leading-edge boundary layer of a swept wing," *Physics of Fluids*, Vol. 33, No. 9, pp. 094111.

Mori, Y., Yakeno, A., Obayashi, S. 2024, " Effects of Surface Roughness and Free-stream Turbulence on Transition in Swept-Wing Boundary Layer", *AIAA Paper*, No. 2024-1565.

Saric, W. S., Carrillo, R. B., Reibert, M. S., 1998, "Leading-Edge Roughness as a Transition Control Mechanism", *AIAA Paper*, No. 98–0781.

Saric, W. S., West, D. E., Tufts, M. W., Reed, H. L., 2015, "Flight Test Experiments on Discrete Roughness Element Technology for Laminar Flow Control", *AIAA Paper*, No. 2015-0539.

Saric, W. S., West, D. E, Tufts, M. W. and Reed, H. L., 2019, "Experiments on Discrete Roughness Element Technology for Swept-Wing Laminar Flow Control", *AIAA Journal*, Vol. 57, No. 2, pp. 641–654.

Ide, Y., Hirota, M. Tokugawa, N., 2021, "Stability assessment on sinusoidal roughness elements for crossflow-transition control", *Physics of Fluids*, Vol. 33, pp. 034112.

Hirota, M., Hattori, Y., Ide, Y., Takami, H., Yoshimoto, M., 2019, "Raised structure and wing, a patent-pending". JP2021-511412, US17/599,092.

Poll, D.I.A., 1979, "Transition in the in finite swept attachment line boundary layer," *Aeronautical Quarterly*, Vol. 30, Issue 4, pp. 607-629.

Gaster, M., 1967, "On the Flow Along Swept Leading Edges", *Aeronautical Quarterly*, Vol. 18, Issue 2, pp. 165-184.

Lynde, M. N., Campbell, R. L., 2017, "Computational Design and Analysis of a Transonic Natural Laminar Flow Wing for a Wind Tunnel Model", *AIAA Paper,* No. 2017-3058.

Paredes, P., Venkatachari, B., 2021, "Transition Analysis for the CRM-NLF Wind Tunnel Configuration", *AIAA Paper*, No. 2021-1431.

Spalart, P. R. and Allmaras, S. R., 1994, "A One-Equation Turbulence Model for Aerodynamic Flows," *Recherche Aerospatiale*, No. 1, 1994, pp. 5-21.

Leer, B. V., 1979, "Towards the ultimate conservative difference scheme, V. A second order sequel to Godunov's method," *Journal of Computational Physics*, 32, pp. 101– 136.

Kermani, M., Gerber, A., Stockie, J., 2003, "Thermodynamically based moisture prediction using roe's scheme," *Proceedings in the 4th Conference of Iranian Aerospace Society*, Amir Kabir University of Technology, Tehran, Iran, Vol. 3.

Nishida, H. and Nonomura, T. 2006 "ADI-SGS Scheme on Ideal Magnetohydrodynamics," *Journal of Computational Physics*, Vol. 228, Issue 9, pp. 3182-3188.

Lynde, M. N., Campbell, R. L. and Viken, S. A., 2019, "Additional findings from the common research model natural laminar flow wind tunnel test," *AIAA Paper*, No. 2019-3292.

Lele, S. K., 1992, "Compact finite difference schemes with spectral-like resolution," *Journal of Computational Physics*, Vol. 103, pp. 16-42.

Gaitonde, D. V., Visbal, M. R., 2000, "Pad ́e-type high-order boundary filters for the Navier-Stokes equations," *AIAA Journal*, Vol. 38, pp. 2103-2112.

Kawai, S., Fujii, K., 2008, "Compact scheme with filtering for large-eddy simulation of transitional boundary layer, " *AIAA Journal*, Vol. 46, pp. 690-700.

Shu, C. W., Osher, S., 1998, "Efficient implementation of essentially non-oscillatory shock capturing schemes, " *Journal of Computational Physics*, Vol. 77, pp. 439-471.